HHS Public Access

Author manuscript

Nat Genet. Author manuscript; available in PMC 2014 August 01.

Published in final edited form as:

Nat Genet. 2014 February ; 46(2): 152–160. doi:10.1038/ng.2853.

Therapeutic modulation of eIF2α-phosphorylation rescues TDP-43 toxicity in amyotrophic lateral sclerosis disease models

Hyung-Jun Kim[1,*], **Alya R. Raphael**[2], **Eva S. LaDow**[3], **Leeanne McGurk**[1], **Ross Weber**[1], **John Q. Trojanowski**[4], **Virginia M.-Y. Lee**[4], **Steven Finkbeiner**[3], **Aaron D. Gitler**[2], and **Nancy M. Bonini**[1]

[1]Department of Biology, University of Pennsylvania, Philadelphia, PA 19104

[2]Department of Genetics, Stanford University School of Medicine, Stanford, CA 94305

[3]Gladstone Institute of Neurological Disease, San Francisco, California 94143

[4]Department of Pathology and Laboratory Medicine, Perelman School of Medicine, Philadelphia, PA 19104

Abstract

Amyotrophic lateral sclerosis (ALS) is a fatal, late-onset neurodegenerative disease primarily impacting motor neurons. A unifying feature of many proteins associated with ALS, including TDP-43 and Ataxin-2, is that they localize to stress granules. Unexpectedly, we found that genes that modulate stress granules are striking modifiers of TDP-43 toxicity in *Saccharomyces cerevisiae* and *Drosophila melanogaster*, eIF2α phosphorylation is upregulated by TDP-43 toxicity in flies, and TDP-43 interacts with a central stress granule component polyA binding protein (PABP). In human ALS spinal cord neurons, PABP accumulates abnormally, suggesting that prolonged stress granule dysfunction may contribute to pathogenesis. We investigated the efficacy of a small molecule inhibitor of eIF2α-phosphorylation in ALS models. This treatment mitigated TDP-43 toxicity in flies and mammalian neurons. These findings indicate that dysfunction induced by prolonged stress granule formation may contribute directly to ALS and that compounds that mitigate this process may represent a novel therapeutic approach.

INTRODUCTION

Amyotrophic Lateral Sclerosis (ALS) is an intractable neurodegenerative disease that affects upper and lower motor neurons, resulting in debilitating and lethal paralysis [1,2]. There is no

Correspondence should be addressed to N.M.B (nbonini@sas.upenn.edu).

*Present address: Convergence Brain Research Department, Korea Brain Research Institute (KBRI), Daegu, South Korea, 700-010

Author Contributions

H.-J.K., A.R.R., E.S.L., L.M., A.D.G. conceived, designed and performed experiments, performed statistical analysis, analyzed data; R.W. performed experiments; J.Q.T, V. M.-Y.L. contributed reagents and materials, and experimental input; S.F., A.D.G., N.M.B. conceived and designed experiments, analyzed data, and supervised the research; H.-J.K., and N.M.B., with input from A.R.R. and A.D.G., wrote the paper.

Financial Disclosures:

A.D.G. is an inventor on patents and patent applications that have been licensed to FoldRx.

cure and only one effective treatment, riluzole, which extends life by only 3 months on average. Thus, novel therapeutic strategies are desperately needed. The genetic underpinnings of sporadic and familial ALS are heterogeneous and incompletely characterized, but almost all cases of ALS share a pathological endpoint: ubiquitin-positive cytoplasmic inclusions that contain the RNA binding protein TDP-43 [3]. Focus on TDP-43 and other RNA-binding proteins has intensified as mutations in members of an expanding family of RNA recognition motif-containing proteins with prion-like domains, FUS/TLS, TAF15, EWSR1, hnRNPA2B1, and hnRNPA1, have been found in ALS patients [4–7]. Efforts to identify the molecular functions of TDP-43 that may be relevant to its role in proteinopathy have elucidated several roles in RNA processing [8], including a possible function in the formation and regulation of RNA granules that form in conditions of stress [9–11].

When primary neurons and cultured cells are stressed, TDP-43 translocates from the nucleus to cytoplasmic stress granules [11,12]. Stress granules are thought to be protective during cellular stress, harboring translationally arrested poly(A)+ mRNA, polyA-binding protein (PABP), 40S ribosomal subunits, and eukaryotic initiation factors [13]. The importance of nuclear-to-cytosolic trafficking of TDP-43 in stressed cells is not yet clear. The parallels between these observations in cells and the cytoplasmic mis-localization of TDP-43 and inclusion formation in patient spinal cord tissue has raised the possibility that stress granule formation may represent sites of early protein aggregation in ALS [14–17]. Prolonged stress granule activity is predicted to lead to a prolonged stressed state and prolonged translational repression, which would be deleterious [15,18–20]. In prion disease models, sustained translational repression by eIF2α phosphorylation mediates neurodegeneration [21,22].

To define toxic features of TDP-43 that may be relevant to human disease, we have used yeast and fly models coupled with human patient tissue analysis. Yeast and fly have proven to be powerful model systems for revealing mechanistic insight into several neurodegenerative diseases, including ALS, Parkinson, Huntington, and Alzheimer diseases [23–28]. High throughput screens in yeast, coupled with functional testing in the *Drosophila* nervous system, have been highly successful at identifying modifiers of disease genes with findings that extend to the human condition [5,25]. Here we find that a genome-wide yeast screen revealed genes in RNA metabolism, including several RNA-binding proteins with connections to stress granules, as critical to TDP-43 toxicity. Pursuing this, we unexpectedly found that eiF2α-phosphorylation, indicative of stress granules and translational repression, becomes abnormally upregulated upon TDP-43-associated neurodegeneration in *Drosophila*, and key genes that modulate eiF2α–phosphorylation dramatically affect the ability of TDP-43 to be neurotoxic. We pursued these studies to reveal a role of polyA binding protein, then extended these studies to show that a small molecule that mitigates eiF2α-phosphorylation may provide a promising avenue for therapeutic intervention in disease.

RESULTS

Yeast reveals a role for stress granule components in ALS

We previously developed a TDP-43 yeast model that recapitulates key features of TDP-43 associated with disease including toxicity and aggregation [29,30]. Using this model, we performed a screen for genes that when upregulated would modify TDP-43 toxicity [25,29–31]. A yeast query strain carrying an integrated copy of TDP-43 under the control of a galactose inducible promoter was transformed with the yeast FLEX gene library, which contains an arrayed set of 5500 genes that are overexpressed upon galactose induction [24,32]. Transformed yeast cells were subsequently plated on glucose (TDP-43 expression OFF) and galactose plates (TDP-43 expression ON), and screened for genes that suppressed or enhanced TDP-43 toxicity. We identified 40 hits, which included 13 suppressors and 27 enhancers of TDP-43 toxicity (Table 1). GO term analysis on the entire set of screen hits showed a striking enrichment in RNA metabolic process, cell cycle, transport and protein modification process genes (Fig. 1a). While there was little overlap between the hits found in this TDP-43 screen and in a previous FUS overexpression screen [33], both screens were enriched for RNA metabolic processes, and to a lesser extent cell cycle genes (Fig. 1a,b). We performed the screen in triplicate, and hits confirmed all three times were independently verified with more sensitive spotting assays (Fig. 1c).

Analysis of the TDP-43 screen hits revealed that stress granule and P-body components (involved in RNA triage and degradation [34]) were significantly enriched (Table 1; 5 out of 40 hits, 12.5%, versus 50 out of 6311 genes in the yeast genome, 0.8%; $P=1x10^{-4}$). These included both enhancers and suppressors of toxicity (Fig. 1b,c). Among the genes was PBP1, the yeast homolog of Ataxin-2, which we previously defined as a protein that synergizes with TDP-43 in promoting toxicity, and whose polyQ repeat expansions are a genetic contributor to ALS [25,35–37]. Because of the importance of RNA metabolic processes in ALS pathogenesis [36] and the enrichment of RNA-binding proteins as modifiers, we performed a network analysis of the identified RNA-binding proteins, defining genetic and physical interactions between hits and additional genes that interacted with the hits (Fig. 1d). Strikingly, this analysis revealed multiple interactions between genes from the screen and *PAB1*, which encodes polyA-binding protein. Additionally, a previously uncharacterized yeast gene, *YGR054W*, was identified as interacting physically and genetically with several of the TDP-43 modifier genes (Fig. 1d); *YGR054W* encodes the yeast homolog of a translation initiation factor EIF2A [38]. This network analysis and the additional interactors predicted by it helped us to focus our further analyses on PAB1 and translation initiation factors (see below).

Given these findings, we then asked whether TDP-43 colocalized with the stress granule marker PUB1. These studies revealed that TDP-43 accumulations in yeast co-localize with PUB1 (Fig. 1e). Stress granule and P-body markers have been found to colocalize with TDP-43 aggregates in patient samples and multiple models of disease [10,39], the results of this unbiased genetic screen indicate that stress granule components, and the stressed state induced by such components, may play a direct role in TDP-43 toxicity, as modifying their expression impacts TDP-43 toxicity. Thus, not only are RNA granules markers of TDP-43

pathology in disease, but they may play a more direct role in neurodegenerative disease pathogenesis.

Stress granule genes modulate TDP-43 toxicity in the fly

To test the significance of the interaction between stress granules and ALS-associated RNA binding protein toxicity in the nervous system, we used *Drosophila*. Although it is challenging to image stress granules *in vivo* in flies, eIF2α-phosphorylation induces the accumulation of non-functional translation initiation complexes that concentrate in stress granules, thus levels of eIF2α-phosphorylation are directly correlated with the levels of stress granules [13]. We extracted protein from heads of control and TDP-43-expressing animals, and immunoblotted extracts with a phospho-specific eIF2α antibody (Ser51). This approach revealed a progressive increase in eIF2α-phosphorylation upon expression of TDP-43 in the brain: there was no difference between control and TDP-43-expressing flies in the levels of eIF2α-phosphorylation at 5d, but by 8d and 14d, the levels of eIF2α-phosphorylation were significantly increased to 1.4±0.1-fold (s.e.m.), and 1.6±0.1-fold (s.e.m.), respectively (Fig. 2a). There was no observed increase in levels of eIF2α protein, showing that the change in phospho-eIF2α levels represented a change in the stress granule specific form (Supplementary Fig. 1). These data suggest that TDP-43 expression in the fly brain induces chronic eIF2α-phosphorylation. Moreover, the increase in eIF2α-phosphorylation indicates a state of prolonged translational repression [22].

To determine whether modulation of this could have an effect on TDP-43-associated neurodegeneration, we examined whether altering the levels of key genes that impact eIF2α-phosphorylation could modulate TDP-43 toxicity *in vivo*. We knocked down the levels of *PEK*, *Rox8*, and *Gadd34* by RNAi in the presence of TDP-43 and examined the progressive effects on TDP-43-induced climbing dysfunction. PEK is the homolog of mammalian PERK and is a kinase that phosphorylates eIF2α, Rox8 is the *Drosophila* homologue of TIA1 which facilitates the physical aggregation of stress granules, and Gadd34 is a phosphatase for eIF2α [40–43]. In mammalian cell lines, loss of *PERK* blocks calcium-induced stress granule formation, stimulation of eIF2α-phosphorylation is necessary and sufficient for stress granule induction [44], expression of dominant negative TIA1 prevents stress granule formation [45], and GADD34 inhibitor treatment induces massive stress granule formation [46]. Thus, reduction of *PEK* and *Rox8* are predicted to inhibit, whereas knockdown of *Gadd34* should enhance, stress granule formation in *Drosophila*.

Flies expressing TDP-43 show a markedly reduced climbing ability compared to normal animals aged to 14d (28±5% (95% CI) compared to 82±5% in controls, Fig. 2b). This climbing deficit was greatly suppressed by knockdown of either *Rox8* or *PEK*, with 62±6% (95%CI) of flies retaining climbing ability; conversely, knockdown of *Gadd34* led TDP-43-expressing flies to lose their motility almost entirely (Fig. 2b). Importantly, we confirmed that downregulation of *PEK* decreased eIF2α-phosphorylation, and that *Gadd34* increased eIF2α-phosphorylation (Fig. 2c). Knockdown of *Gadd34*, *PEK* or *Rox8* on their own had no effect on climbing abillity (data not shown). Intriguingly, *Gadd34* reduction, which enhanced TDP-43 toxicity in our locomotion assay, also led to accumulation of TDP-43 protein in the cytoplasm (Fig. 2d). Taken together, these data indicate that TDP-43-induced

neural toxicity can be dramatically enhanced and suppressed by altering genes that converge on eIF2α phosphorylation.

The TDP-43/Ataxin-2 interaction requires the PAM2 motif

To provide more insight into this potentially critical role of stress granules in TDP-43 toxicity, we investigated in greater detail the interaction between Ataxin-2 and TDP-43. Ataxin-2, like TDP-43, localizes to stress granules and regulates their assembly and functions [47,48]. PolyQ expansions in Ataxin-2 are a risk for ALS, and the Ataxin-2 protein has several functional motifs including one for the key stress granule protein, PolyA Binding Protein (PABP) [49]. We generated transgenic fly lines that express human Ataxin-2 with a normal length polyQ repeat (ATXN2-22Q), or an expanded repeat within the risk range for ALS (ATXN2-32Q). As with fly Ataxin-2 [25], co-expression of either protein with TDP-43 dramatically enhanced toxicity, with faster loss of lifespan and climbing ability (Supplementary Fig. 2). Intriguingly, ATXN2-32Q enhanced the toxicity of TDP-43 measured by lifespan more significantly than ATXN2-22Q, demonstrating that an expansion of only ten glutamine repeats from normal into the ALS-associated range has a significant effect *in vivo.*

Ataxin-2 has two key domains implicated in RNA binding function (Fig. 3a): the Lsm (like Sm) domain is important for RNA binding affinity [50], whereas the PAM2 motif mediates interaction with PABP [51]. We generated domain deletion forms of ATXN2-32Q and selected transgenic lines that express these proteins at the same level as intact ATXN2-32Q. Expression of the deletion-bearing ATXN2-32Q proteins alone showed effects comparable to the intact ATXN2-32Q protein: a mild disruption of retinal structure and slightly reduced lifespan (Supplementary Fig. 3). When we then assessed the ability of these forms to enhance toxicity of TDP-43. Strikingly, whereas the ATXN2-Q32-ΔLSM protein acted the same as ATXN2-Q32, the ATXN2-32Q-ΔPAM2 protein completely lost the ability to interact with TDP-43 in retinal toxicity (Fig. 3b-c). These results were similar for lifespan and climbing ability, with the ATXN2-32Q-ΔPAM2 form showing almost complete loss of interaction with TDP-43 (Fig. 3). TDP-43 protein accumulation was also unaffected by ATXN2-32Q-ΔPAM2 (Fig. 3e), consistent with functional loss of the interaction. This finding raised the possibility that PABP, which binds the PAM2 motif, may have a role in TDP-43-induced neurodegeneration and that the shared interaction of TDP-43 and Ataxin-2 with PABP may represent a critical axis in stress granule formation and the biological effects of that stress.

Poly-A binding protein modulates TDP-43 toxicity in *Drosophila*

To investigate the potential role of PABP in ALS-associated gene toxicity, we examined the effects of the fly gene *dPABP* (the *Drosophila* homologue of the cytoplasmic protein PABPC1) on toxicity of TDP-43 and ATXN2. Whereas upregulation of *dPABP* on its own had minimal effects, co-expression with either TDP-43 or ATXN2-32Q enhanced toxicity, resulting in more severe retinal degeneration (Fig. 4a). Consistent with a role for dPABP in conveying toxicity due to the interaction of TDP-43 with ATXN2, dPABP did not modulate ATXN2-32Q-ΔPAM2 (Fig. 4a). The effect of *dPABP* on TDP-43 was exquisitely dose-dependent: reduction of endogenous levels using RNAi significantly delayed the progressive

loss of motility that occurs upon expression of TDP-43 in the nervous system (Fig. 4b). *dPABP* downregulation did not impact total TDP-43 protein levels in the brain, but did cause a reduction to 0.7±0.1 (s.e.m.) fold of the cytoplasmic levels of TDP-43, compared to TDP-43 with normal *dPABP* levels (Fig. 4c). Consistent with the essential function of the RNA binding activity of TDP-43, expression of TDP-43 with point mutations in the aromatic residues of the RNA-recognition motifs (RRMs) [25,52] failed to induce neurodegeneration or synergize with ATXN2 or *dPABP* (Supplementary Fig. 4). We confirmed that *dPABP* had no effect on the efficiency of the GAL4/UAS driver system (Supplementary Fig. 5). These data indicate that interactions with PABP modulate TDP-43 toxicity, suggesting that PABP function may be critical in human disease.

PABPC1 is mislocalized in spinal cord motor neurons in ALS

To determine if PABP function may be altered in human disease, we immunostained control and ALS patient spinal cord tissue for PABPC1 protein, the cytoplasmic PABP, to examine whether there were pathological associations between PABPC1 localization and ALS disease. In control spinal cord neurons, PABPC1 shows a diffuse cytoplasmic localization pattern in most neurons (Fig. 5a), occasionally being present in denser accumulations (2±0.7% (s.e.m.) motor neurons, Fig. 5b, 5e). In ALS patient spinal cord tissue, robust cytoplasmic inclusions of PABPC1 were observed in 13±4% (s.e.m.) of motor neurons (Fig. 5c-e; Supplementary Table 1). Recent analysis of co-localization pathological phosphorylated TDP-43 with PABPC1 indicated ~70% overlap in ALS human tissues [10]. These data suggest that interactions with or altered function of PABPC1 may occur in ALS disease, and that these punctate accumulations containing PABPC1 in ALS spinal cords may represent structures with a functional role similar to that of stress granules, and be indicative of a prolonged stress state and associated altered signaling pathways. Taken together, these findings raised the possibility that treatment approaches that alter activities that impact stress granules, and their contingent effects on translation and signaling pathways, may impact ALS disease progression.

Pharmacologic rescue of TDP-43 toxicity

To test the idea that targeting eIF2α-phosphorylation in a therapeutic manner may modulate TDP-43 toxicity in the nervous system, we turned back to the fly. Our data with gene manipulation indicated that inhibition of PEK activity might be effective to mitigate TDP-43 toxicity. Compounds that inhibit PERK, the human homologue of PEK, have been developed. We therefore tested whether treating flies with the PERK inhibitor compound GSK2606414 [53] could impact TDP-43-associated neurodegeneration. Flies fed 10uM GSK2606414 showed a markedly reduced level of eIF2a-phosphorylation, to 63±3% (s.e.m.) of that in heads of TDP-43-expressing animals (Fig. 6a). Remarkably, at this level of treatment, there was a dramatic mitigation of TDP-43-induced climbing dysfunction: whereas normally at 12d, TDP-43-expressing flies had only 18±5% (95% CI) climbing ability, with inhibitor treatment they now retained 42±7% (95% CI) climbing ability (Fig. 6b).

To extend these studies to the mammalian neurons, we assessed the ability of the PERK inhibitor to mitigate toxicity of TDP-43 to primary neurons. Rat primary cortical neurons

were transfected with two constructs: one expressing mApple, and the other expressing either enhanced green florescent protein (EGFP) alone or EGFP tagged TDP-43. We imaged ~800–1000 individual neurons from each condition at 24-hr intervals for 7d using automated microscopy [54]. Death of neurons was scored by the loss of detectable cell body mApple fluorescence. Previous studies have shown that upregulation of TDP-43 is toxic to neurons, inducing degeneration, cytoplasmic mislocalization of TDP-43 and aggregation of the protein [55], thus reflecting fundamental features of pathological TDP-43 associated with disease. To then assess the ability of GSK2606414 to mitigate TDP-43 toxicity, we first performed a dose-response to the compound, testing a range of compound concentrations (100, 250, 500nM, 1, 2, 5 uM). Concentrations of 1 uM or higher were deleterious on their own, but the nM concentrations were tolerated (Fig. 6d-e; Supplementary Table 2). We thus assessed the effect of compound on TDP-43 toxicity with concentrations of 100, 250 and 500 nM. These studies showed that treatment of primary neurons with PERKi GSK2606414 mitigated TDP-43 toxicity at 250 and 500 nM ($p<0.01$, Fig. 6e, Supplementary Table 2c). Taken together, these data indicate that prolonged activity of eIF2α-phosphorylation functionally impacts TDP-43 toxicity, and suggest the possibility that compounds that mitigate this, such as GSK2606414, could be developed as a therapeutic strategy for ALS and related TDP-43 proteinopathies.

DISCUSSION

A common biological feature of several RNA-binding proteins connected to neurodegenerative diseases is their localization to cytoplasmic stress granules, and a working hypothesis for disease is that stress granule formation facilitates or promotes TDP-43 aggregation in ALS [11,15,17–20,39] Moreover, stress granule markers such as TIA1 and eIF3 co-localize with TDP-43 inclusions in ALS and the clinicopathologically-related disorder, FTLD-U [16]. However, the relationship between these observations and neurotoxicity is not clear. These findings do suggest, however, that ALS may be associated with a prolonged stress state and the outcome of such a state. Thus, it has been unclear whether genes that impact stress granule formation could directly affect TDP-43 neurotoxicity. The impact of prolonged stress granules would long-term translational repression and altered signalling pathways; sustained translational repression is thought to be causal in prion-mediated neurodegeneration and mitigating this has an effect to mitigate disease [21,22]. Here, we show that eIF2α-phosphorylation is increased upon TDP-43-induced neural dysfunction in *Drosophila*, that genes that are implicated in stress granule formation impact TDP-43 toxicity in yeast, and that TDP-43 induced climbing deficits are mitigated by knockdown of genes whose activity normally modulates eIF2α-phosphorylation. Moreover, the interaction between Ataxin-2 and TDP-43 is mediated through PABP, which is mislocalized in ALS. As a proof of principle that modulating eIF2α-phosphorylation could be beneficial, a small molecule inhibitor of PERK activity significantly suppressed TDP-43 toxicity *in vivo* in the fly, and mitigated TDP-43 toxicity to mammalian primary cortical neurons. Thus, inhibitory activity of molecules on stress granule formation, and thus on a potentially prolonged stress state in disease, may accurately gauge potential therapeutic activity *in vivo*. Molecules that decrease stress granule formation or stability could be a promising treatment avenue for ALS and other TDP-43 proteinopathies. Such compounds

may affect TDP-43 accumulation, and also mitigate the outcome of prolonged stress on cells that contributes to their degeneration.

Online Methods

Yeast Plasmid Overexpression Screen

The query strain was generated by integrating TDP-43 into the *HIS3* locus using a p303-GAL-TDP-43 vector [25]. Plasmids from the yeast FLEXgene collection (5500 full-length yeast ORFs) were transformed into the query strain. The screen was performed similarly to previous screens [33] and as described [25,31]. The screen was replicated three times and only those hits that consistently reproduced were considered to be modifiers of TDP-43. A control strain with YFP (p303-GAL-YFP) integrated into the *HIS3* locus was used in experiments to confirm that the overexpression strains did not lead to toxicity or a growth advantage when expressed in the absence of TDP-43. GO-term analysis of the hits was performed using the GO-slim mapper tool available at the SGD website, www.yeastgenome.org. GeneMANIA [56] was used to search for interacting genes based physical and genetic interactions.

Yeast Transformation and Spotting Assays

PEG/Lithium acetate yeast transformations and spotting assays were performed according to standard protocols.

Visualizing Stress Granules in Yeast

A plasmid expressing PUB1-mCherry, a stress granule marker [57], was transformed into the wild type yeast strain BY4741. Subsequently, p415-GAL-GFP or p415-GAL-TDP-43-GFP plasmids were transformed into the strain. The TDP-43 expression plasmid was created using an LR reaction with the destination vector p415-GAL-ccdB-GFP and the donor vector pDONR221-TDP-43 (CCSB Human ORFeome Collection).

Transformants were grown overnight in raffinose-containing selective media (CSM-Ura-Leu) and then added to galactose-containing selective media and allowed to grow for 6 hours to induce the expression of the galactose inducible genes. Yeasts were mounted in the media they were growing in on coverslips coated with concanavalin A (Sigma #L7647) [58]. Images were captured on a Leica DM6000B with a ProEM EMCCD camera (Princeton Instruments).

Fly strains

Drosophila stocks were maintained on standard cornmeal agar media at 25°C unless otherwise noted. *elav*^{3A}*–GAL4* was a gift from Mark A. Tanouye [59]. *UAS-TDP-43* is described previously [25]. The Bloomington stock center provided other fly stocks.

DNA constructs for germ line transformation

For generating random insertion transgenic lines, we used the pUAST vector [60]. Human ATXN2 cDNA that has 32 CAG repeats was cloned into pUAST vector as BglII-XbaI fragments. The pUAST-ATXN2-Q32-ΔPAM2 construct was generated by deleting the

region encoding amino acids 910-922 of the PAM2 domain. The pUAST-ATXN2-32Q construct containing encoding the full length ATXN2 protein with 32Q repeats was used as a template for two PCR reactions. The region 5′ of the PAM2 domain was amplified using a forward primer containing an attached *Bgl*II cut site primer PAM2-N1 (primer sequences listed in Supplementary Table 3) and a reverse primer complimentary to the beginning of the PAM2 domain and containing an attached *Hind*III cut site primer PAM2-N2. The region 3′ of the PAM2 domain was amplified using a forward primer complimentary to the end of the PAM2 domain and containing an attached *Hind*III cut site primer PAM2-C1 and a reverse primer containing an attached *Xba*I cut site primer PAM2-C2. Each PCR product was subcloned into TOPO vectors, cloned into pUAST vectors, cut out of the pUAST vector, ligated together, and reinserted into a pUAST vector.

Similarly, the pUAST-ATXN2-Q32-ΔLSM construct was generated by deleting the region encoding amino acids 267-325 of the PAM2 domain. The pUAST-ATXN2-Q32 construct was used as a template for two PCR reactions. The region 5′ of the LSM domain was amplified using a forward primer containing an attached *Bgl*II cut site primer LSM-N1 and a reverse primer complimentary to the beginning of the LSM domain and containing an attached *Hind*III cut site primer LSM-N2. The region 3′ of the LSM domain was amplified using a forward primer complimentary to the end of the LSM domain and containing an attached *Hind*III cut site primer LSM-C1, and a reverse primer containing an attached *Xba*I cut site primer LSM-C2. Each PCR product was subcloned into TOPO vectors, cloned into pUAST vectors, cut out of the pUAST vector, ligated together, and reinserted into a pUAST vector.

For generation of site-specific integration transgenic lines, we used pJFRC5 and pJFRC5-myc vector [61]. ATXN2 cDNAs that with 32 CAG or 22 CAG repeats were cloned into pJFRC5-myc vector as *Swa*I-*Xba*I fragment. These DNA constructs were integrated into the attP2 landing site.

External eye and retinal tissue microscopy

For fly eye pictures, we used a Leica Z16-Apo A motorized zoom microscope system with DFC420 digital camera and Leica Application Suite Montage module software (Leica Microsystems). Retinal tissue was visualized by autofluorescence in horizontal paraffin sections. 0-1d males were used for experiments.

Lifespan and adult climbing assays

0-1d males were separated and transferred onto experimental vials containing fly media mixed with or without RU486 (20μg/ml or 40μg/ml) at a density of 20 (for life span) or 25 (for climbing assay) flies per vial. Dead flies were scored everyday and flies were transferred to fresh media every other day. All flies for climbing assays or life span analysis raised at 29°C. Adult locomotor function was assessed by a previously described method, with 125 flies per genotype per time point in all experiments, except for SFig. 2d where 150 flies per genotype per time point were used [62]. Experiments were repeated twice to assure consistent results.

Western immunoblotting

For total protein extraction, 10 male fly heads were homogenized in 1X LDS sample buffer (Invitrogen). For subcellular fractionation, 20 male fly heads were lysed in NE-PER extraction reagent (Pierce) according to the manufacturer's protocol. The extracts (equivalent to 2 heads/lane) were then run on 3–8% Tris Acetate gel or 4–12% Bis-Tris gel (Invitrogen). Western blotting was performed according to standard protocols. The following primary antibodies were used: anti-TDP-43 (1:800, Proteintech, catalog # 10782-2-AP); anti-β-Actin (1:2000, Abcam, catalog # ab16039); anti-α-Tubulin (1:2000, conjugated with HRP, Cell Signaling, catalog # 9099); anti-Lamin C (1:1000, Deveopmental Studies Hybridoma Bank, catalog # LC28.26); anti-phospho-eIF2α (1:1000, Cell signaling tech, Catalog #9722); anti-mouse-Ataxin-2 (1:300, BD biosciences, catalog # 6113378), anti-rabbit-eIF2α (1:1000, Abcam, catalog # ab26197) and anti-mouse β-galactosidase (Promega, catalog # Z3781). After incubation with HRP-coupled secondary antibodies (goat anti-rabbit diluted 1:2000 and goat anti-mouse diluted 1:2000; Pierce), blots were visualized using ECL plus or prime kit (Amersham Biosciences). Quantification of Western blots was performed using ImageGauge4.22 (GE Healthcare).

Immunohistochemistry of human post-mortem spinal cord

Human spinal cord tissue fixed in 10% neutral buffered formalin was processed into paraffin wax. The tissue was cut into 7 μm sections and PABPC1 was immunolocalized with antigen retrieval (Antigen unmasking solution, citric acid based, Vector Laboratories, catalog # H-3300) and the avidin-biotin complex detection method with 3,3-diaminobenzidine as the chromagen (Vectastain ABC detection kit, Vector Labs, catalog # PK-6100). PABPC1 rabbit polyclonal antibody was used at 1:800 (Cell Signaling, catalog # 4992S). Biotinylated anti-rabbit IgG (Vector Labs, catalogue #: BA-1000) was used at 1:1000. Stained sections were counterstained with hematoxylin and eosin.

Drug treatment

GSK2606414 (PERK inhibitor, EMD Millipore, catalog #: 516535) was added directly to media from a 1mg/ml stock (dissolved in DMSO) to give final concentration 10μM. The same amount of DMSO was added for vehicle control.

Statistical analyses

For climbing and immunoblot quantifications, data were analyzed by Student's *t*-test (Vassar Stats, www.vassarstats.net) or first analyzed using one-way ANOVA followed by Tukey's multiple comparisons test (GraphPad Prism Software, La Jolla, CA). Human immunohistochemistry data was analyzed by one-tailed Mann-Whitney test (VassarStats). Differences were considered significant when $p<0.05$, and are indicated as follows: * $p<0.05$; ** $p<0.01$; *** $p<0.001$; # $p<0.0001$; n.s., not significant.

Plasmids

For primary cell culture, human TDP43 was cloned into pGW1-CMV plasmid, C-terminally fused to EGFP as described [55]. EGFP and mApple were cloned into pGW1-CMV as described [55,63].

Cell culture

Cortical neurons were isolated from E20-21 Long Evans rat embryos (Charles River) and cultured at 100,000 cells/well of 96 well plate in serum-free Neurobasal medium (Invitrogen) supplemented with B27, GlutaMax, and pen/strep (Invitrogen). At 4d *in vitro* (DIV), neurons were transfected with Lipofectamine 2000 (Invitrogen) per manufacturers protocol. Neurons were cotransfected with plasmids encoding survival markers (mApple) or proteins of interest (TDP43-EGFP or EGFP control) in a 1:1 molar ratio for a total of 0.2 μg total DNA per well. After transfection cells were returned to Neurobasal media mixed 1:1 with conditioned media. For cells treated with PERK inhibitor (GSK2606414, CalBiochem), drug was added once immediately after transfection.

Robotic microscopy

For neuronal survival analysis, we use a robotic imaging system as described [63]. Briefly, images are obtained with an inverted Nikon microscope (Ti-E) equipped with PerfectFocus, an extra-long working distance (ELWD) 20x objective lens, and a back-illuminated Andor iXON 888 14-bit, cooled, electron multiplying charge coupled device (EMCCD). Illumination is provided a xenon lamp and liquid light guide. All movements of the stage are controlled with electrical stepper motors. Coordination of fluorescence excitation and emission filters, stage movements, focusing, and imaging acquisition are accomplished with custom-designed and commercially available programs.

Image analysis and statistics

Digitized images were assembled into montages in Pipeline Pilot and ImageJ using original programs. Background fluorescence from neighboring regions of interest was subtracted, montages from each time point are assembled into stacks in chronological order and aligned with one another. Cell bodies of transfected neurons, identified by morphology marker fluorescence (mApple), were automatically segmented and followed over time. Cell death was determined by an abrupt loss of fluorescence, indicating shrinkage or disappearance of the cell body. The time of death for each neuron was considered the last time that the neuron was present. Kaplan-Meier and cumulative risk of death curves were generated in R. Statistical significance of survival differences between cohorts of neurons is determined by the log-rank test, and Cox proportional hazards analysis used to measure the relative change in the risk of death attributed to various experimental conditions.

Supplementary Material

Refer to Web version on PubMed Central for supplementary material.

Acknowledgments

We thank Xiuyin Teng and Dr. Yongqing Zhu for technical assistance, Dr. William Motley, Dr. Amit Berson and other laboratory members for insightful comments. This work was funded by grants from the Howard Hughes Medical Institute (N.M.B.), R01NS073660 (A.D.G. and N.M.B.), NIH Director's New Innovator Award DP2OD004417 (A.D.G.) and R01NS065317 (A.D.G.), the Robert Packard Center for ALS and the Williams H. Adams Foundation (S.F.), and AG10124, AG32953, AG17586 and NS53488 (J.Q.T. and V.M.-Y.L.). A.D.G. and S.F. are supported by a grant from Target ALS. A.R.R. is supported by a BrightFocus Alzheimer's disease research grant.

References

1. Boillee S, Vande Velde C, Cleveland DW. ALS: a disease of motor neurons and their nonneuronal neighbors. Neuron. 2006; 52:39–59. [PubMed: 17015226]
2. Cleveland DW, Rothstein JD. From Charcot to Lou Gehrig: deciphering selective motor neuron death in ALS. Nat Rev Neurosci. 2001; 2:806–19. [PubMed: 11715057]
3. Al-Chalabi A, et al. The genetics and neuropathology of amyotrophic lateral sclerosis. Acta Neuropathol. 2012; 124:339–52. [PubMed: 22903397]
4. Couthouis J, et al. Evaluating the role of the FUS/TLS-related gene EWSR1 in amyotrophic lateral sclerosis. Hum Mol Genet. 2012; 21:2899–911. [PubMed: 22454397]
5. Couthouis J, et al. A yeast functional screen predicts new candidate ALS disease genes. Proc Natl Acad Sci U S A. 2011; 108:20881–90. [PubMed: 22065782]
6. Kim HJ, et al. Mutations in prion-like domains in hnRNPA2B1 and hnRNPA1 cause multisystem proteinopathy and ALS. Nature. 2013
7. King OD, Gitler AD, Shorter J. The tip of the iceberg: RNA-binding proteins with prion-like domains in neurodegenerative disease. Brain Res. 2012; 1462:61–80. [PubMed: 22445064]
8. Warraich ST, Yang S, Nicholson GA, Blair IP. TDP-43: a DNA and RNA binding protein with roles in neurodegenerative diseases. Int J Biochem Cell Biol. 2010; 42:1606–9. [PubMed: 20601083]
9. Aulas A, Stabile S, Vande Velde C. Endogenous TDP-43, but not FUS, contributes to stress granule assembly via G3BP. Mol Neurodegener. 2012; 7:54. [PubMed: 23092511]
10. Bentmann E, et al. Requirements for stress granule recruitment of fused in sarcoma (FUS) and TAR DNA-binding protein of 43 kDa (TDP-43). J Biol Chem. 2012; 287:23079–94. [PubMed: 22563080]
11. Parker SJ, et al. Endogenous TDP-43 localized to stress granules can subsequently form protein aggregates. Neurochem Int. 2012; 60:415–24. [PubMed: 22306778]
12. Dewey CM, et al. TDP-43 is directed to stress granules by sorbitol, a novel physiological osmotic and oxidative stressor. Mol Cell Biol. 2011; 31:1098–108. [PubMed: 21173160]
13. Thomas MG, Loschi M, Desbats MA, Boccaccio GL. RNA granules: the good, the bad and the ugly. Cell Signal. 2011; 23:324–34. [PubMed: 20813183]
14. Hart MP, Gitler AD. ALS-associated ataxin 2 polyQ expansions enhance stress-induced caspase 3 activation and increase TDP-43 pathological modifications. J Neurosci. 2012; 32:9133–42. [PubMed: 22764223]
15. Li YR, King OD, Shorter J, Gitler AD. Stress granules as crucibles of ALS pathogenesis. J Cell Biol. 2013; 201:361–72. [PubMed: 23629963]
16. Liu-Yesucevitz L, et al. Tar DNA binding protein-43 (TDP-43) associates with stress granules: analysis of cultured cells and pathological brain tissue. PLoS One. 2010; 5:e13250. [PubMed: 20948999]
17. Wolozin B. Regulated protein aggregation: stress granules and neurodegeneration. Mol Neurodegener. 2012; 7:56. [PubMed: 23164372]
18. Bentmann E, Haass C, Dormann D. Stress granules in neurodegeneration--lessons learnt from TAR DNA binding protein of 43 kDa and fused in sarcoma. FEBS J. 2013; 280:4348–70. [PubMed: 23587065]
19. Ramaswami M, Taylor JP, Parker R. Altered Ribostasis: RNA-Protein Granules in Degenerative Disorders. Cell. 2013; 154:727–36. [PubMed: 23953108]
20. Thomas M, Alegre-Abarrategui J, Wade-Martins R. RNA dysfunction and aggrephagy at the centre of an amyotrophic lateral sclerosis/frontotemporal dementia disease continuum. Brain. 2013; 136:1345–60. [PubMed: 23474849]
21. Moreno JA, et al. Oral Treatment Targeting the Unfolded Protein Response Prevents Neurodegeneration and Clinical Disease in Prion-Infected Mice. Sci Transl Med. 2013; 5:206ra138.
22. Moreno JA, et al. Sustained translational repression by eIF2alpha-P mediates prion neurodegeneration. Nature. 2012; 485:507–11. [PubMed: 22622579]

23. Auluck PK, Chan HY, Trojanowski JQ, Lee VM, Bonini NM. Chaperone suppression of alpha-synuclein toxicity in a Drosophila model for Parkinson's disease. Science. 2002; 295:865–8. [PubMed: 11823645]
24. Cooper AA, et al. Alpha-synuclein blocks ER-Golgi traffic and Rab1 rescues neuron loss in Parkinson's models. Science. 2006; 313:324–8. [PubMed: 16794039]
25. Elden AC, et al. Ataxin-2 intermediate-length polyglutamine expansions are associated with increased risk for ALS. Nature. 2010; 466:1069–75. [PubMed: 20740007]
26. Gitler AD, et al. Alpha-synuclein is part of a diverse and highly conserved interaction network that includes PARK9 and manganese toxicity. Nat Genet. 2009; 41:308–15. [PubMed: 19182805]
27. Outeiro TF, Lindquist S. Yeast cells provide insight into alpha-synuclein biology and pathobiology. Science. 2003; 302:1772–5. [PubMed: 14657500]
28. Treusch S, et al. Functional links between Abeta toxicity, endocytic trafficking, and Alzheimer's disease risk factors in yeast. Science. 2011; 334:1241–5. [PubMed: 22033521]
29. Johnson BS, McCaffery JM, Lindquist S, Gitler AD. A yeast TDP-43 proteinopathy model: Exploring the molecular determinants of TDP-43 aggregation and cellular toxicity. Proc Natl Acad Sci U S A. 2008; 105:6439–44. [PubMed: 18434538]
30. Johnson BS, et al. TDP-43 is intrinsically aggregation-prone, and amyotrophic lateral sclerosis-linked mutations accelerate aggregation and increase toxicity. J Biol Chem. 2009; 284:20329–39. [PubMed: 19465477]
31. Armakola M, Hart MP, Gitler AD. TDP-43 toxicity in yeast. Methods. 2011; 53:238–45. [PubMed: 21115123]
32. Hu XH, et al. Genetic dissection of ethanol tolerance in the budding yeast Saccharomyces cerevisiae. Genetics. 2007; 175:1479–87. [PubMed: 17194785]
33. Sun Z, et al. Molecular determinants and genetic modifiers of aggregation and toxicity for the ALS disease protein FUS/TLS. PLoS Biol. 2011; 9:e1000614. [PubMed: 21541367]
34. Jain S, Parker R. The discovery and analysis of P Bodies. Adv Exp Med Biol. 2013; 768:23–43. [PubMed: 23224963]
35. Lagier-Tourenne C, Polymenidou M, Cleveland DW. TDP-43 and FUS/TLS: emerging roles in RNA processing and neurodegeneration. Hum Mol Genet. 2010; 19:R46–64. [PubMed: 20400460]
36. Ling SC, Polymenidou M, Cleveland DW. Converging mechanisms in ALS and FTD: disrupted RNA and protein homeostasis. Neuron. 2013; 79:416–38. [PubMed: 23931993]
37. Tazen S, et al. Amyotrophic Lateral Sclerosis and Spinocerebellar Ataxia Type 2 in a Family With Full CAG Repeat Expansions of ATXN2. JAMA Neurol. 2013
38. Zoll WL, Horton LE, Komar AA, Hensold JO, Merrick WC. Characterization of mammalian eIF2A and identification of the yeast homolog. J Biol Chem. 2002; 277:37079–87. [PubMed: 12133843]
39. Dewey CM, et al. TDP-43 aggregation in neurodegeneration: are stress granules the key? Brain Res. 2012; 1462:16–25. [PubMed: 22405725]
40. Anderson P, Kedersha N. Visibly stressed: the role of eIF2, TIA-1, and stress granules in protein translation. Cell Stress Chaperones. 2002; 7:213–21. [PubMed: 12380690]
41. Brand S, Bourbon HM. The developmentally-regulated Drosophila gene rox8 encodes an RRM-type RNA binding protein structurally related to human TIA-1-type nucleolysins. Nucleic Acids Res. 1993; 21:3699–704. [PubMed: 8396236]
42. Dalton LE, Healey E, Irving J, Marciniak SJ. Phosphoproteins in stress-induced disease. Prog Mol Biol Transl Sci. 2012; 106:189–221. [PubMed: 22340719]
43. Khong A, Jan E. Modulation of stress granules and P bodies during dicistrovirus infection. J Virol. 2011; 85:1439–51. [PubMed: 21106737]
44. Kimball SR, Horetsky RL, Ron D, Jefferson LS, Harding HP. Mammalian stress granules represent sites of accumulation of stalled translation initiation complexes. Am J Physiol Cell Physiol. 2003; 284:C273–84. [PubMed: 12388085]
45. Kedersha N, et al. Dynamic shuttling of TIA-1 accompanies the recruitment of mRNA to mammalian stress granules. J Cell Biol. 2000; 151:1257–68. [PubMed: 11121440]

46. Ruggieri A, et al. Dynamic oscillation of translation and stress granule formation mark the cellular response to virus infection. Cell Host Microbe. 2012; 12:71–85. [PubMed: 22817989]
47. Nonhoff U, et al. Ataxin-2 interacts with the DEAD/H-box RNA helicase DDX6 and interferes with P-bodies and stress granules. Mol Biol Cell. 2007; 18:1385–96. [PubMed: 17392519]
48. Swisher KD, Parker R. Localization to, and effects of Pbp1, Pbp4, Lsm12, Dhh1, and Pab1 on stress granules in Saccharomyces cerevisiae. PLoS One. 2010; 5:e10006. [PubMed: 20368989]
49. Kozlov G, Menade M, Rosenauer A, Nguyen L, Gehring K. Molecular determinants of PAM2 recognition by the MLLE domain of poly(A)-binding protein. J Mol Biol. 2010; 397:397–407. [PubMed: 20096703]
50. Chowdhury A, Raju KK, Kalurupalle S, Tharun S. Both Sm-domain and C-terminal extension of Lsm1 are important for the RNA-binding activity of the Lsm1–7-Pat1 complex. RNA. 2012; 18:936–44. [PubMed: 22450758]
51. Satterfield TF, Pallanck LJ. Ataxin-2 and its Drosophila homolog, ATX2, physically assemble with polyribosomes. Hum Mol Genet. 2006; 15:2523–32. [PubMed: 16835262]
52. Buratti E, Baralle FE. Characterization and functional implications of the RNA binding properties of nuclear factor TDP-43, a novel splicing regulator of CFTR exon 9. J Biol Chem. 2001; 276:36337–43. [PubMed: 11470789]
53. Axten JM, et al. Discovery of 7-methyl-5-(1-{[3-(trifluoromethyl)phenyl]acetyl}-2,3-dihydro-1H-indol-5-yl)-7H-p yrrolo[2,3-d]pyrimidin-4-amine (GSK2606414), a potent and selective first-in-class inhibitor of protein kinase R (PKR)-like endoplasmic reticulum kinase (PERK). J Med Chem. 2012; 55:7193–207. [PubMed: 22827572]
54. Arrasate M, Mitra S, Schweitzer ES, Segal MR, Finkbeiner S. Inclusion body formation reduces levels of mutant huntingtin and the risk of neuronal death. Nature. 2004; 431:805–10. [PubMed: 15483602]
55. Barmada SJ, et al. Cytoplasmic mislocalization of TDP-43 is toxic to neurons and enhanced by a mutation associated with familial amyotrophic lateral sclerosis. J Neurosci. 2010; 30:639–49. [PubMed: 20071528]
56. Zuberi K, et al. GeneMANIA prediction server 2013 update. Nucleic Acids Res. 2013; 41:W115–22. [PubMed: 23794635]
57. Hofmann S, Cherkasova V, Bankhead P, Bukau B, Stoecklin G. Translation suppression promotes stress granule formation and cell survival in response to cold shock. Mol Biol Cell. 2012; 23:3786–800. [PubMed: 22875991]
58. Buchan JR, Yoon JH, Parker R. Stress-specific composition, assembly and kinetics of stress granules in Saccharomyces cerevisiae. J Cell Sci. 2011; 124:228–39. [PubMed: 21172806]
59. Hekmat-Scafe DS, Dang KN, Tanouye MA. Seizure suppression by gain-of-function escargot mutations. Genetics. 2005; 169:1477–93. [PubMed: 15654097]
60. Brand AH, Perrimon N. Targeted gene expression as a means of altering cell fates and generating dominant phenotypes. Development. 1993; 118:401–15. [PubMed: 8223268]
61. Pfeiffer BD, et al. Refinement of tools for targeted gene expression in Drosophila. Genetics. 2010; 186:735–55. [PubMed: 20697123]
62. Feany MB, Bender WW. A Drosophila model of Parkinson's disease. Nature. 2000; 404:394–8. [PubMed: 10746727]
63. Arrasate M, Finkbeiner S. Automated microscope system for determining factors that predict neuronal fate. Proc Natl Acad Sci U S A. 2005; 102:3840–5. [PubMed: 15738408]

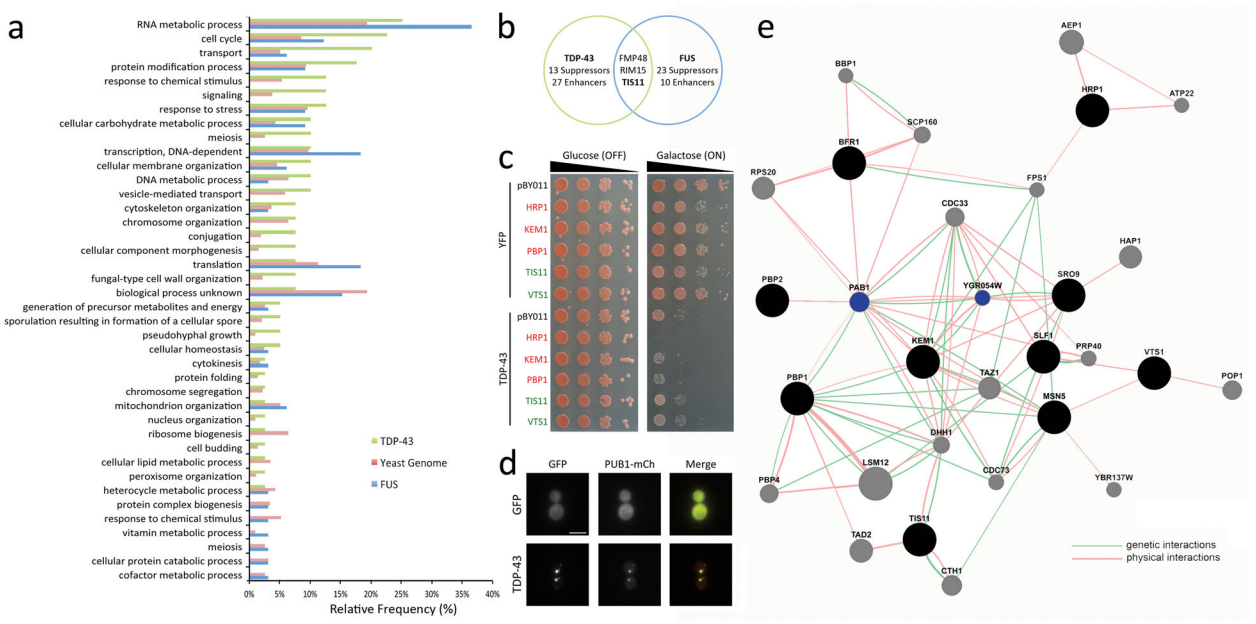

Figure 1. Yeast plasmid overexpression screen highlights the role of stress granules in TDP-43 toxicity

a) Histogram showing the functional categories of genes (GO term process) with the relative frequency of genes from the TDP-43 overexpression screen compared to the yeast genome and to the FUS overexpression screen [33]. Both the TDP-43 and FUS screens were enriched for RNA metabolic process genes, while the TDP-43 screen was enriched for cell cycle, transport, and protein modification process genes.

b) While the TDP-43 and FUS screens were both enriched for RNA metabolic process genes, most of the hits did not overlap with the exception of three genes.

c) Stress granule genes identified in the screen enhance or suppress TDP-43 toxicity. Spotting assay showing that on the galactose plate (expression ON) the co-expression of HRP1, KEM1, or PBP1 with TDP-43 leads to enhanced toxicity (reduced growth) while the co-expression of TIS11 or VTS1 with TDP-43 leads to suppression of toxicity (increased growth).

d) RNA-binding protein focused yeast interaction network for TDP-43 screen hits reveal connections to PAB1 and EIF2A homolog. Ten out of forty yeast genes that modified TDP-43 toxicity when overexpressed are annotated as RNA-binding proteins. These are displayed as black circles. GeneMANIA [56] was used to search for interacting genes based physical and genetic interactions. Interacting genes are displayed as grey circles and network edges are colored based on the type of interaction (red=physical interaction and green=genetic interaction). This analysis revealed strong connections to PAB1 and YGR054W, which are highlighted in blue. YGR054W is the yeast homolog of a human translation initiation factor EIF2A.

e) GFP-tagged ALS-linked disease gene TDP-43 forms aggregates when expressed in yeast that colocalize with the stress granule marker PUB1-mCherry. Scale bar, 5 μm.

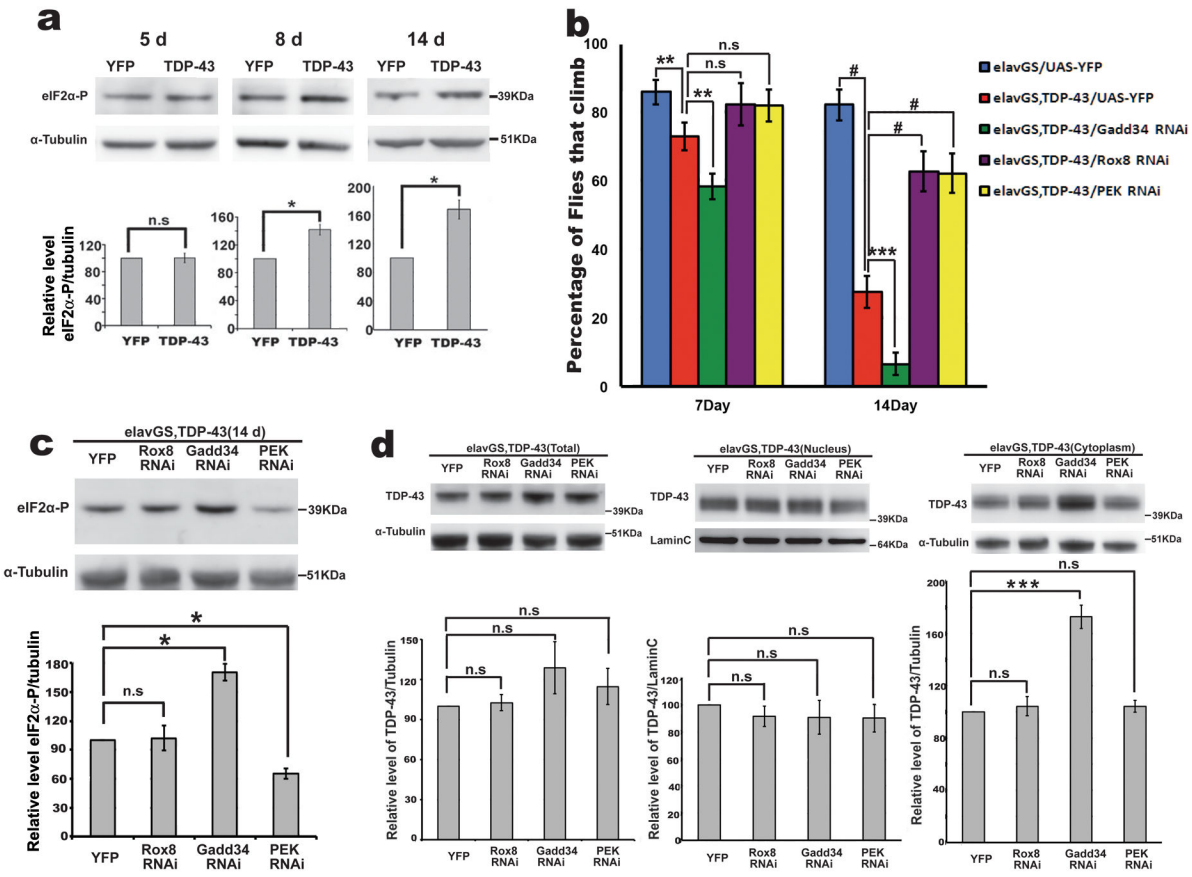

Figure 2. Genes that impact stress granule formation modulate TDP-43 toxicity

a) TDP-43 expression increases eIF2α-phosphorylation levels. Genes were expressed in the nervous system in a drug-inducible manner with the elavGS driver. eIF2α- phosphorylation level of elavGS/UAS-YFP and elavGS, TDP-43/UAS-YFP flies fed as adults on RU486 (40μg/ml), and assessed at the indicated time-points. Genotypes: Control is *elav*GS/*UAS-YFP*. TDP-43 is *elav*GS, *UAS-TDP-43(S)/UAS-YFP*. Mean ± s.e.m., n=3 independent experiments. *p<0.05, *** p<0.001, n.s., not significant. (Student's *t*-test).

b) Altering the levels of genes that reduce stress granule formation mitigates TDP-43 toxicity, and that promote stress granule formation enhances TDP-43 toxicity. Mean ± 95% CI of four experiments. Genotypes: elavGS/UAS-YFP is *elavGS/UAS-YFP*. elavGS, TDP-43/UAS-YFP is *elav*GS, *UAS-TDP-43(S)/UAS-YFP*. elavGS, TDP-43/Gadd34 RNAi is *elav*GS, *UAS-TDP-43(S)/UAS-Gadd34. RNAi*^{HMS00811}. elavGS, TDP-43/Rox8 RNAi is *elav*GS, *UAS-TDP-43(S)/UAS-Rox8. RNAi*^{HMS00472}. elavGS, TDP-43/PEK RNAi is *elav*GS, *UAS-TDP-43(S)/UAS-PEK. RNAi*^{GL00030}. All flies raised with RU486 (40μg/ml) (125 flies per genotype). ANOVA for significance, followed by Tukey's multiple comparison test, **p<0.01, *** p<0.001, # p<0.0001, n.s., not significant.

c) eIF2α-phosphorylation level of elavGS, TDP-43/UAS-YFP, elavGS, TDP-43/Rox8 RNAi, elavGS, TDP-43/Gadd34 RNAi and elavGS, TDP-43/PEK RNAi. Mean ± s.e.m., n=3 independent experiments. *p<0.05, n.s., not significant (Student's *t*-test).

d) Total, nuclear and cytosolic TDP-43 protein level in 10d fly heads. Genes predicted to increase stress granules formation increase cytoplasmic TDP-43 protein levels. Mean ± s.e.m., n=3 independent experiments. *** $p<0.001$, n.s., not significant (Student's *t*-test).

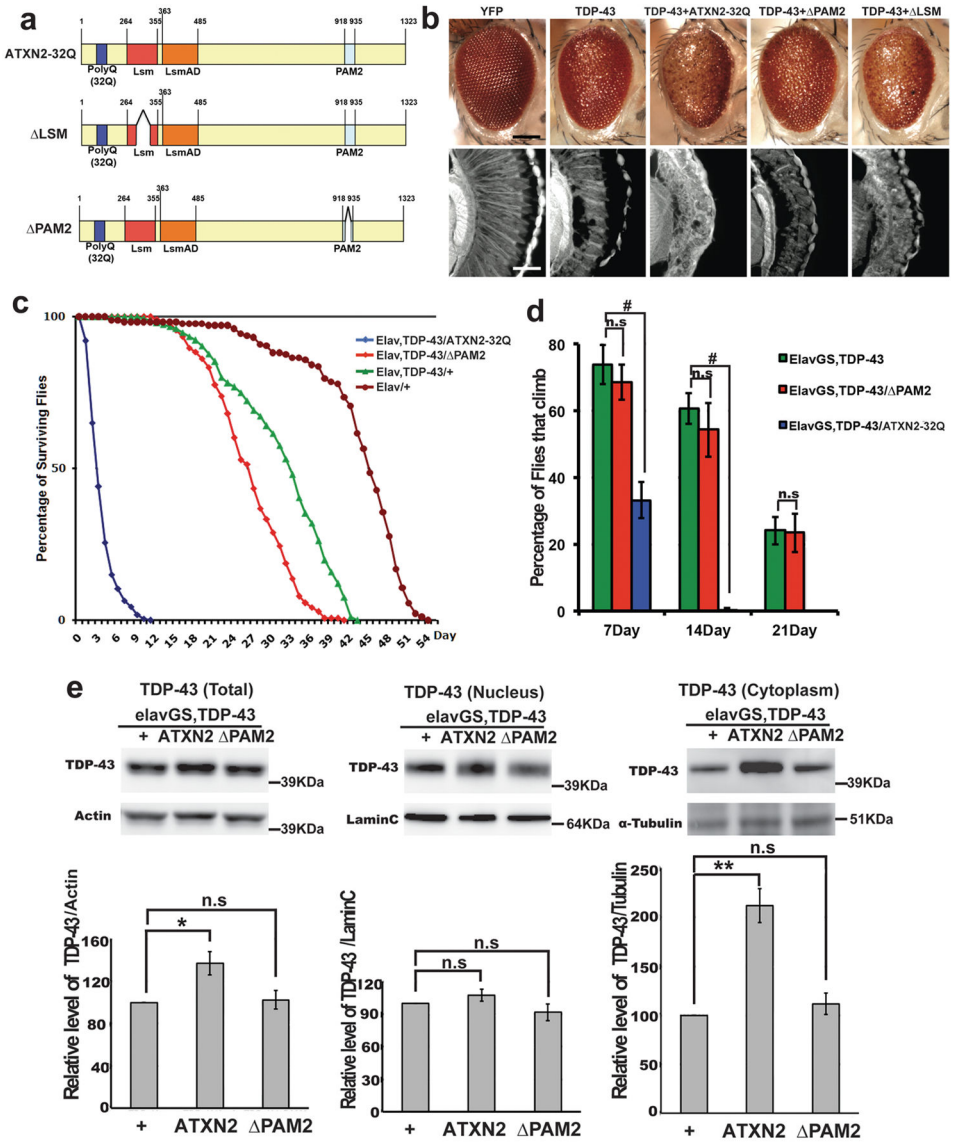

Figure 3. The interaction between TDP-43 and Ataxin-2 is mediated through the polyA binding protein motif of Ataxin-2

a) Schematic representation of the versions of Ataxin-2 generated and tested for interactions with TDP-43. Colored boxes indicate the putative RNA-binding Lsm domain, the Lsm-associated domain LsmAD, the PABP-interacting motif PAM2 and the polyQ stretch. Deletion region of ΔLSM is aa277-346, and ΔPAM2 is aa920-932 of ATXN2-32Q. Both domains are well conserved from yeast to mammal.

b) TDP-43 toxicity is not affected by co-expression of ATXN2 lacking the PAM2 motif. Whereas TDP-43 toxicity is enhanced with co-expression of ATXN2-32Q or ATXN2-32Q-ΔLSM (TDP-43+ATXN2-32Q or TDP-43+ΔLSM), there is no effect with co-expression of ATXN2-32Q-ΔPAM2 (TDP-43+ΔPAM2). Genotypes: YFP is *gmr-GAL4(YH3)/UAS-YFP*. TDP-43 is *UAS-TDP-43(M)/+; gmr-GAL4(YH3)/+*. TDP-43+ATXN2-32Q is *UAS-TDP-43(M)/+; gmr-GAL4(YH3)/UAS-ATXN2-32Q*. TDP-43+ΔPAM2 is *UAS-TDP-43(M)/+; gmr-GAL4(YH3)/UAS-ATXN2-32Q.ΔPAM2*. TDP-43+ΔLSM is *UAS-*

TDP-43(M)/+; gmr-GAL4(YH3)/UAS- ATXN2-32Q.ΔLSM. Scale bar for eyes, 100 μm; for sections, 10 μm.

c) Expression of TDP-43 in the nervous system reduces lifespan (green, compared with normal in brown). Expression of ATXN2-32Q greatly enhanced TDP-43 toxicity (blue), but the ATXN2-32Q.ΔPAM2 deletion mutant form did not (red). Genotypes: Elav/+ is *elav*^{3A}*-GAL4/+* (n=177 flies). Elav, TDP-43/+ is *elav*^{3A}*-GAL4, UAS-TDP-43(S)/+* (n=156). Elav, TDP-43/ATXN2-32Q is *elav*^{3A}*-GAL4, UAS-TDP-43(S)/UAS-ATXN2-32Q* (n=152). Elav, TDP-43/ΔPAM2 is *elav*^{3A}*-GAL4, UAS-TDP-43(S)/UAS-ATXN2-32Q.* Δ*PAM2* (n=138).

d) TDP-43 caused progressive loss of climbing ability when expressed in the adult nervous system (green) which is dramatically enhanced by co-expression of ATXN2-32Q (blue). However, the ΔPAM2 form of ATXN2-Q32 has little effect (red) compared to TDP-43 alone. Mean ± 95% CI of four experiments (n=125 flies per genotype). # $p<0.0001$, n.s., not significant (ANOVA for significance, followed by Tukey's multiple comparison test).

e) Total, nuclear and cytosolic TDP-43 protein levels in 10d fly heads. Cytosolic TDP-43 protein level is greatly increased by ATXN2-32Q; ΔPAM2 expression does not affect TDP-43 localization or level. Mean ± s.e.m., n=3-4. # $p<0.0001$, n.s., not significant (ANOVA for significance, followed by Tukey's multiple comparison test).

d–e Genotypes: elavGS, TDP-43/+ is *elavGS, UAS-TDP-43(S)/+*.elavGS, TDP-43/ ATXN2-32Q is *elav*GS, *UAS-TDP-43(S)/ UAS-ATXN2-32Q.* elavGS, TDP-43/ΔPAM2 is *elav*GS, *UAS-TDP-43(S)/ UAS-ATXN2-32Q.*Δ*PAM2.* All flies raised with RU486 (20 μg/ ml). *$p<0.05$, **p< 0.01, n.s. not significant. (ANOVA for significance, followed by Student's *t*-test).

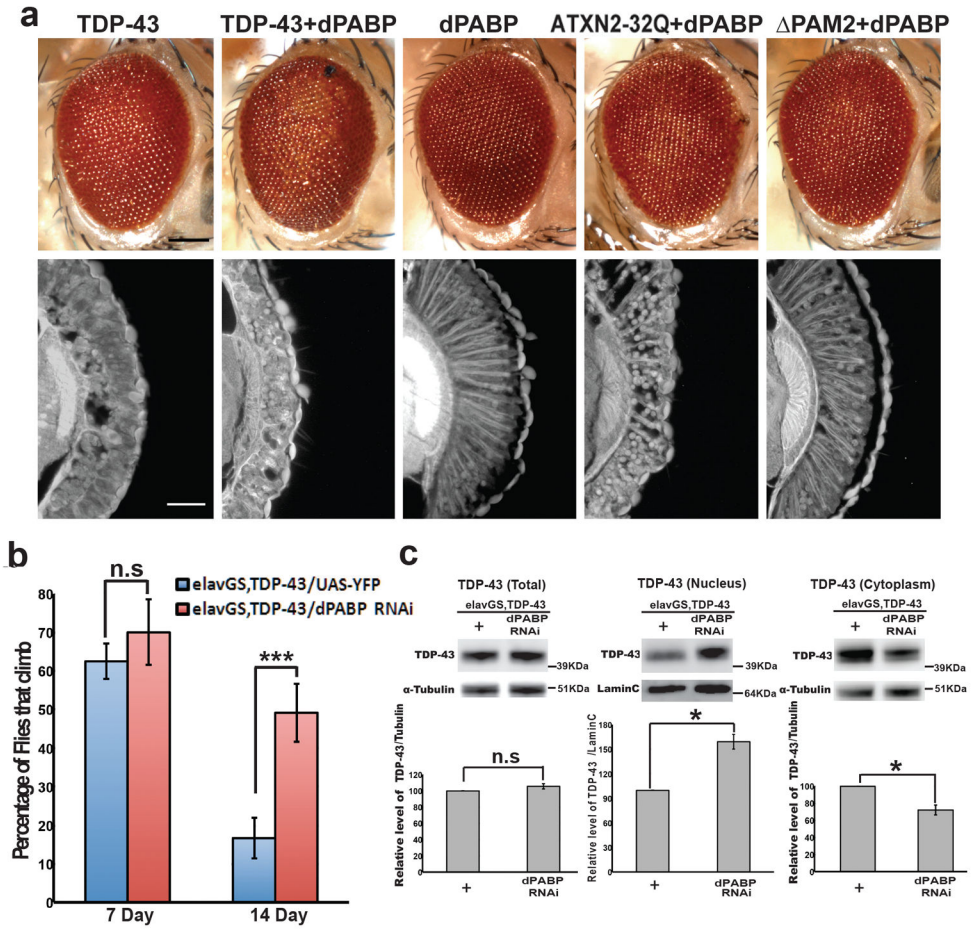

Figure 4. Poly(A) binding protein is required for TDP-43 toxicity

a) dPABP upregulation enhances TDP-43 and ATXN2-32Q toxicity. However, dPABP does not interact with the ΔPAM2 form of ATXN2-32Q. Genotype: TDP-43 is *UAS-TDP-43(M)/+; gmr-GAL4(YH3)/+*. TDP-43+dPABP is *UAS-TDP-43(M)/+; gmr-GAL4(YH3)/UAS-dPABP*. PABP is *gmr-GAL4(YH3)/UAS-dPABP*. ATXN2-32Q+dPABP is *gmr-GAL4(YH3), UAS-dPABP/ UAS-ATXN2-32Q*.ΔPAM2+dPABP is *gmr-GAL4(YH3), UAS-dPABP/ UAS-ATXN2-32Q.ΔPAM2*. Scale bar for eyes, 100 μm; for sections, 10 μm.

b) TDP-43 loss of climbing ability is suppressed by downregulation of dPABP. Genotypes: elavGS, TDP-43/+ is *elavGS, UAS-TDP-43(S)/+*. elavGS, TDP-43/dPABP RNAi is *elavGS, UAS-TDP-43(S)/UAS-dPABP.RNAi*^{JF03104} (125 flies/genotype). Mean ± 95% CI of four experiments. *** $p<0.001$, n.s. not significant (Student's *t*-test).

c) Total, nuclear and cytosolic TDP-43 protein levels in 10d fly heads. PABP downregulation decreases cytosolic TDP-43 protein level. Genotype: elavGS, TDP-43/+ is *elav*GS, *UAS-TDP-43(S)/+*. elavGS, TDP-43/dPABP. RNAi is *elavGS, UAS-TDP-43(S)/ UAS-dPABP.RNAi*^{JF03104}. Mean ± s.e.m., n=3 independent experiments *** $p<0.001$, n.s. not significant (Student's *t*-test).

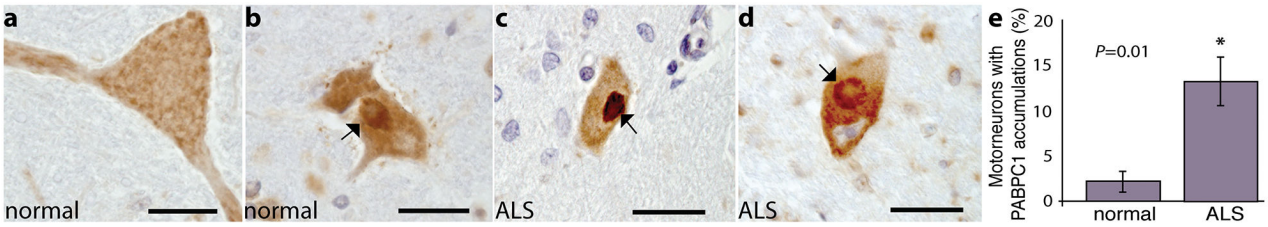

Figure 5. PABPC1 is mislocalized in motor neurons from ALS patient tissue

a–d, Immunostaining for PABPC1 in the cervical spinal cord of control and ALS patients.

a) PABPC1 is expressed in spinal cord motor neurons, and is localized throughout the cytoplasm in a diffuse pattern.

b) Occasionally PABPC1 cytoplasmic accumulations were observed in normal motorneurons (arrow).

c) In ALS patient motor neurons, PABPC1 is present in distinct cytoplasmic and dense accumulations (arrow).

d) PABPC1 cytoplasmic accumulations were also observed in the ALS motorneurons where there was a clearing in the middle. Scale bars, 30 μm.

e) The number of motor neurons containing cytoplasmic accumulation of PABPC1 in ALS patients was significantly greater (p=0.01, one-tailed Mann-Whitney test) than in motor neurons from controls. For quantification of accumulations of PABPC1 in individual normal versus ALS cases, see Supplementary Table 1. n=5 controls, 4 ALS patients, mean ± s.e.m.

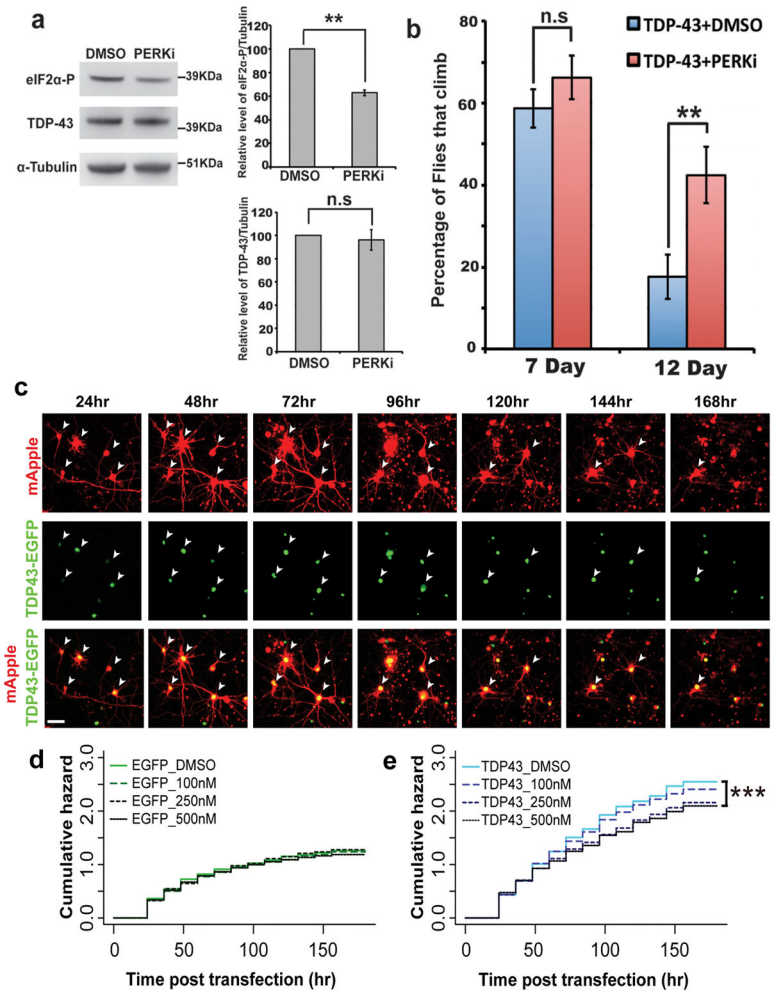

Figure 6. PERK inhibitor treatment rescues TDP-43 toxicity in *Drosophila* and primary rat neurons

a,b, PERK inhibitor reduces eIF2α-phosphorylation levels and mitigates TDP-43 toxicity to flies.

a) Immunoblot of flies expressing TDP-43 in the nervous system. PERK inhibitor decreases eIF2α-phosphorylation levels, but not TDP-43 protein levels. Quantification performed on 3 independent experiments, normalized to tubulin. Mean ± s.e.m. $^{**}p<0.01$, n.s., not significant (Student's *t*-test).

b) Flies expressing TDP-43 by elav were treated with DMSO or PERK inhibitor (GSK2606414,10μM). Genotypes: *elav*^{3A}*-GAL4, UAS-TDP-43(S)/UAS-YFP*. Mean ± s.e.m. n=4 experiments. $^{**}p<0.01$, n.s., not significant (Student's *t*-test).

c-f, PERK inhibitor (PERKi) reduces TDP43 toxicity in primary rat cortical neurons.

c) Representative micrographs showing longitudinal imaging of primary cortical neurons transfected with mApple as morphology marker and TDP43-EGFP. White arrows show cells still counted as alive in survival analysis. Cells were transfected at 4 DIV; hr indicate imaging time post transfection. Scale bar, 20μM.

d-e) Cumulative hazard plots for survival analysis performed on primary cortical neurons treated with PERKi and transfected with mApple and **d**) EGFP, **e**) TDP43-EGFP. PERKi

treatment (500nM) of neurons expressing TDP43-EGFP decreased the risk of death by 14%, compared to neurons expressing TDP43-EGFP with vehicle (DMSO) only treatment. Three independent experiments were analyzed to determine statistical significance and cumulative hazard plots. Statistics was performed by Cox proportional hazards analysis; see Supplementary Table 2 for cells per condition and hazard ratios. *, $p<0.05$. **, $p<0.01$. ***, $p<0.001$. #, $p<0.0001$. n.s., not significant.

Table 1

Genes that suppress or enhance TDP-43 toxicity in yeast when overexpressed

Effect	Gene	Human Homolog	Description
Suppressor	ADY3	CENPE	Protein wall formation
Suppressor	BFR1		Component of mRNP complexes associated with polyribosomes
Suppressor	CYC8		Transcription co-repressor; part of complex that recruits SWI/SNF and SAGA complexes to promoters
Suppressor	FMP48	STK36	Protein of unknown function
Suppressor	HSP104		Heat shock protein chaperon
Suppressor	ICS2		Protein of unknown function
Suppressor	NNK1	DCLK1	Protein kinase; interacts with TORC1, Ure2p and Gdh2p
Suppressor	PGM1	PGM1	Phosphoglucomutase
Suppressor	RDR1		Transcriptional repressor
Suppressor	RIM15	STK38	Glucose-repressible protein kinase
Suppressor	TIS1	ZNF36/TTP	mRNA-binding protein; component of stress granules
Suppressor	VTS1	SAM4B/Smaug	RNA-binding protein containing a SAM domain; component of P granules
Suppressor	XRS2		Protein required for DNA repair
Enhancer	CDC6	CDC6	Essential ATP-binding protein required for DNA replication
Enhancer	DIP5	SLC7A7	Dicarboxylic amino acid permease
Enhancer	HRP1	Musashi 1 & 2	RNA binding protein; component of stress granules
Enhancer	KEL1	RAB9	Protein required for proper cell fusion and cell morphology
Enhancer	KEM1	XRN1	5′-3′ exonuclease component of P bodies
Enhancer	KIN3	NEK2	Serine/threonine protein kinase
Enhancer	MEC1	ATR	Genome integrity checkpoint protein
Enhancer	MSA1	Mucin 17	Involved in regulation of timing of G1-specific gene transcription and cell cycle initiation
Enhancer	MSN5	XPO5	Karyopherin involved in nuclear import and export
Enhancer	MTH1		Negative regulator of the glucose-sensing signal transduction pathway
Enhancer	PBP1	Ataxin 2	Interacts with Pab1p; component of stress granules
Enhancer	PBP2	PCBP1, 2, 3, & 4	RNA binding protein
Enhancer	PCL6		Pho85p cyclin of the Pho80p subfamily
Enhancer	PIB2	WDFY3	Protein binding phosphatidylinositol 3-phosphate
Enhancer	RGA2	ARHGAP15	GTPase-activating protein for Cdc42p
Enhancer	ROM2	NET1	GDP/GTP exchange protein (GEP) for Rho1p and Rho2p
Enhancer	SAK1	CAMKK1	Upstream kinase for the SNF1 complex
Enhancer	SFG1		Putative transcription factor
Enhancer	SLF1	LARP1	RNA binding protein that associates with polysome
Enhancer	SLG1		Sensor-transducer of the stress-activated PKC-MPK1 kinase pathway
Enhancer	SOL1	PGLS	Protein with possible role in tRNA transport
Enhancer	SRO9	LARP2	RNA-binding protein that associates with translating ribosomes
Enhancer	TSC11	RICTOR	Subunit of TORC2
Enhancer	UBP7	USP21	Ubiquitin-specific protease
Enhancer	VHS1	MARK2	Cytoplasmic serine/threonine kinase
Enhancer	YCK2	CSNK1G2	Casein kinase 1 isoform

Effect	Gene	Human Homolog	Description
Enhancer	YHR131C		Putative protein of unknown function

Descriptive information from the *Saccharomyces* Gene Database, www.yeastgenome.org